JOURNAL OF MATERIALS SCIENCE 26 (1991) 5203–5211

Liquid-phase sintering of high-speed steels

J. D. BOLTON, A. J. GANT, R. J. M. HAGUE
Department of Mechanical Engineering, University of Bradford, Bradford BD7 1DP, West Yorkshire, UK

Attempts were made to reduce the sintering temperature required to densify two different grades of high-speed steel by the introduction of copper–phosphorus to promote liquid-phase sintering and by adding carbon to lower the solidus temperature. The use of nitrogen-atmosphere sintering in an effort to lower the sintering temperature through absorption of interstitial nitrogen into the steel did not succeed. Copper–phosphorus combined with carbon additions was successful in reducing sintering temperatures by approximately 100 °C but was more effective in the M3/2 (molybdenum) than in the BT6 (tungsten grade) steels. Densification via a liquid-phase sintering mechanism occurs in a number of stages as different liquid phases are produced by interaction between the copper–phosphorus and the steel. Growth of carbides by solution and reprecipitation due to the transport of alloying elements through these liquid phases is suggested as a major densification process.

1. Introduction

High-speed steel cutting tools produced by the powder metallurgy route are both well known and well documented. Problems arise in using sintered high-speed steels for other wear-resistant applications where high-volume component production is required, e.g. automotive components, because of the use of a vacuum and the need for high sintering temperatures. Normal high-speed steels sintered by conventional means are produced by vacuum batch furnace sintering at temperatures within the range 1250 to 1330 °C and cannot be easily manufactured at high production rates in continuous link belt furnaces, which are incapable of operating at temperatures much above 1150 °C.

The purpose of this experimental work was to determine possible ways of lowering the sintering temperature (needed to produce good density) to a level where high-speed steels could be sintered in a continuous furnace, e.g. sintering at 1150 °C. Two broad approaches were used to achieve a reduction in sintering temperature, the first being to promote liquid-phase sintering through the introduction of phosphorus; the second was to reduce the temperature for super-solidus sintering by lowering the liquidus–solidus temperatures in the high-speed steel. This was attempted by the introduction of extra carbon at the powder mixing stage and by introducing interstitial nitrogen from a controlled sintering atmosphere.

2. Experimental procedure

Sintering trials were carried out with two different grades of water-atomized high-speed steel powder, namely M3 class 2 molybdenum grade and BT6 tungsten grade steel. Both were supplied in the annealed condition and had average particle sizes of around 45 μm. The compositions for each of the two steels are shown in Table I.

The phosphorus addition used to promote liquid phase sintering was added to each of these steels in the form of 7 wt % of copper phosphide powder. This quantity, which was designed to provide a total nominal phosphorus content of 1 wt % within each steel mixture, gave a slightly higher atomic concentration of phosphorus in the BT6 alloys. Additional carbon (0.25 wt %) was also added to some batches of powder in the form of graphite powder. These mixtures were blended by dry mixing in a Y-cone blender for 15 min.

Green compacts for the sintering trials were produced by cold pressing, without lubricant, at a pressure of 800 MPa to form blanks 15 mm square by 4 mm deep. At this pressure the M3/2 steel powder pressed to about 76% of full density whereas the BT6 material only achieved about 73% full density.

Sintering of the green compacts was carried out in a choice of different sintering atmospheres consisting of high vacuum (0.15 μbar), or high-purity, oxygen-free nitrogen at either a partial pressure of 5 torr or at full atmospheric pressure. Heating and cooling conditions were identical for all specimens: the heating cycle consisted of heating to the desired sintering temperature at 10 °C min^{-1} followed by a natural furnace-cool after the sample had been held for a fixed period at the sintering temperature. Both isochronal (for a fixed 30 min) and isothermal sintering treatments were carried out on the two different types of high-speed steel.

Density measurements to assess sintering behaviour were carried out by lacquer-coating the sample to seal surface porosity, followed by weighing to determine the water displacement (Archimedes method). Corrections were made for both the weight and volume of lacquer used.

0022–2461/91 $03.00 + .12

TABLE I Composition of water-atomized high-speed steel powders

Grade	Composition (wt %)						
	C	Co	Cr	Mo	V	W	O
M3/2	1.10	–	4.02	5.8	2.91	6.05	0.09
BT6	0.83	11.5	4.40	–	0.60	20.50	0.04

Monitoring of the pressure during vacuum sintering was used to indicate some of the reactions which occurred during the sintering cycle, e.g. the formation of liquid phases, and this was further reinforced by differential thermal analysis (DTA) of compacted samples using a Stanton Redcroft instrument under either argon or nitrogen atmospheres.

Characterization of sintered microstructures, including the analysis and identification of phases formed by sintering, was carried out by both optical microscopy and scanning electron microscopy with energy-dispersive analysis.

3. Results

3.1. Sintering data

The densification behaviours for isochronal sintering at different temperatures in both M3/2 and BT6 grade high-speed steels are shown in Figs 1 and 2. All curves shown were for steel containing the copper-phosphorus alloy sintering aid, but data points for both vacuum and nitrogen-atmosphere sintering were included on each of the two curves, depending on whether the samples contained additional carbon or not. The data are shown plotted in terms of a shrinkage parameter (change in density relative to initial green density), and as the absolute density. For vacuum sintering without carbon addition it was readily apparent that both the M3/2 and BT6 steels develop distinctive changes in densification rate at set temperature intervals; three step-like increases in densification rate were identified at successively higher sintering temperatures. Also apparent from these data was the fact that carbon addition shifted the sintering curve towards lower temperatures; the effect being most evident for the M3/2 high-speed steel. Sintering within a nitrogen atmosphere produced little obvious change in sintering temperature; the data points for nitrogen-atmosphere sintering tended to lie on the vacuum sintering curves but were displaced depending on the presence or absence of added carbon in the original sample.

Isothermal sintering data obtained by vacuum sintering are shown in Figs 3 and 4. The data were plotted in accordance with the Kingery model [1] for liquid-phase sintering, log(shrinkage) versus log(time), and gave rise to different slopes depending on the sintering temperature. In M3/2-based materials the slope was approximately 1/5 for sintering temperatures between 1085 and 1120 °C and changed to a slope of 1/3 at the lower sintering temperature of 1050 °C. Slope values of approximately 1/5 were recorded for BT6-based material when sintered at

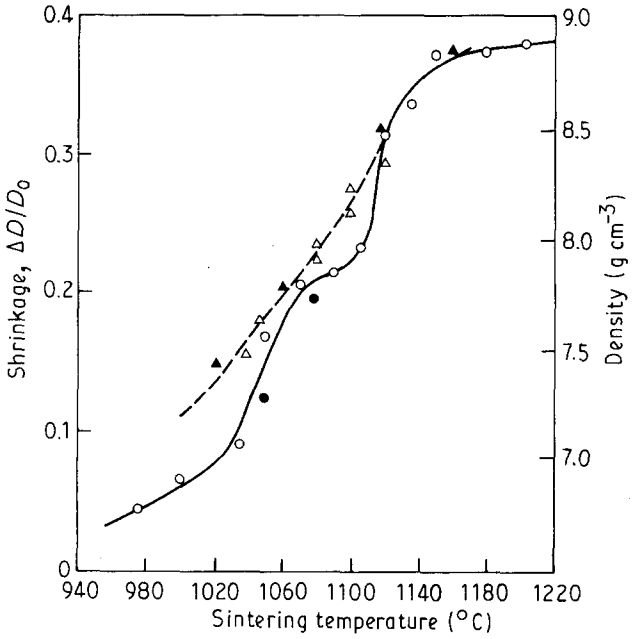

Figure 1 Density versus sintering temperature for BT6 H.S.S. containing 7% copper phosphide both with and without added carbon. No carbon: (○) vacuum, (●) nitrogen. 0.25% C: (△) vacuum, (▲) nitrogen.

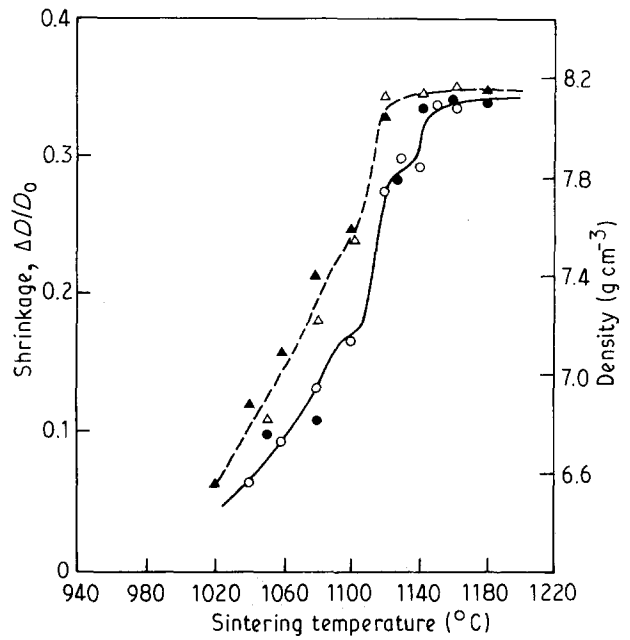

Figure 2 Density versus sintering temperature for M3/2 H.S.S. containing 7% copper phosphide both with and without added carbon. No carbon: (○) vacuum, (●) nitrogen. 0.25% C: (△) vacuum, (▲) nitrogen.

1040 °C, but a much shallower slope of 1/24 occurred at the higher sintering temperature, 1150 °C.

3.2. Phase reactions

Indications of the presence of liquid phases and an associated increase in outgassing rates led to sharp rises in vacuum pressure during vacuum sintering at certain temperatures, as shown in Fig. 5. These curves indicated that liquid phases may have occurred at various temperatures during the heating stage of the

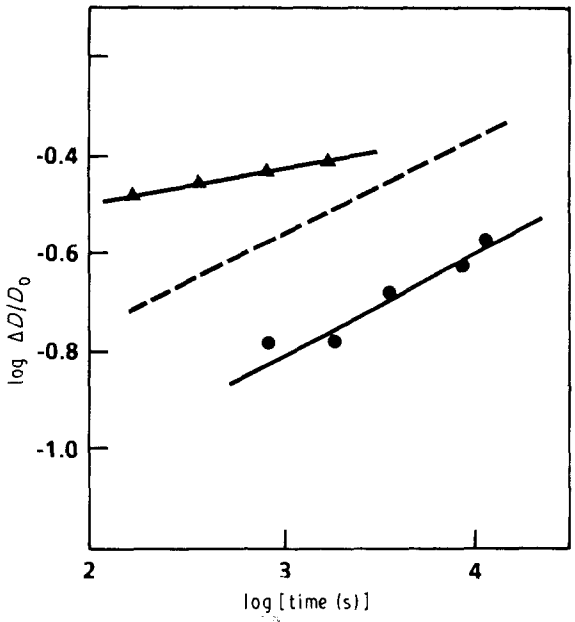

Figure 3 Log(shrinkage) (change in density relative to original green density) versus log(time): BT6 + 7% copper phosphide alloy. (●) 1040 °C, (▲) 1150 °C; (---) line of slope 1/5.

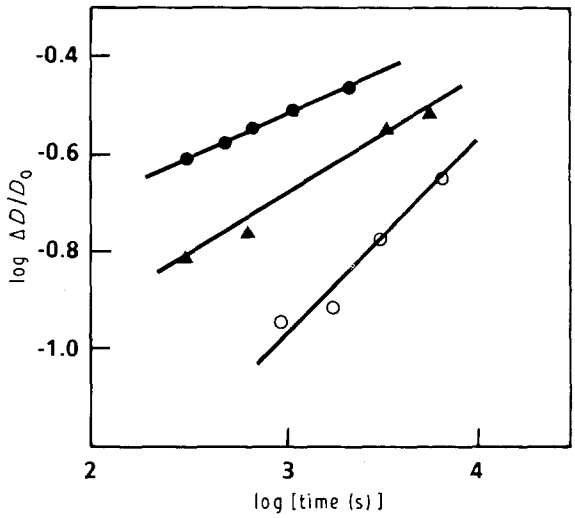

Figure 4 Log(shrinkage) (change in density relative to original green density) versus log(time): M3/2 + 7% copper phosphide alloy. (○) 1050 °C, (▲), 1085 °C, (●) 1120 °C.

sintering treatment. A succession of liquid-phase reactions occurred in both BT6 and M3/2-based samples, where the reaction temperature depended on the presence of added carbon. Typical reaction temperatures which could indicate liquid-phase formation are shown in Table II.

These results show that differences exist between BT6 and M3/2 materials in the way that liquid phases occur: the evidence suggests that a liquid phase begins to appear at a much lower temperature in BT6 than in M3/2 materials, and three rather than two liquids may occur during heating of the BT6-based alloy. In both alloys, carbon can be seen to lower all but the highest of the reaction temperatures, this last temperature being virtually unaffected and remaining at approximately 1085 °C.

TABLE II Liquid-phase reaction temperatures as indicated by gas evolution during vacuum sintering

Alloy	Gas evolution peaks (liquid reaction temperatures) (°C)		
BT6/Cu–P/no added carbon	992	1045	1086
BT6/Cu–P/with added carbon	980	1006	1085
M3/2/Cu–P/no added carbon	–	1054	1086
M3/2/Cu–P/ with added carbon	–	1029	1090

Evidence was also obtained to support these findings from DTA, which confirmed that the gas peaks indicated by Fig. 5 were indeed caused by the formation of a liquid phase. Endothermic peaks due to liquid-phase formation caused by melting occurred during the heating cycle, at very similar temperatures to those shown by Table II, and typical DTA curves are shown in Fig. 6.

The DTA curves also provided evidence of additional reactions: an exothermic reaction was detected at around 710 °C for both BT6 and M3/2-based materials, and liquid phase formation at above 1150 °C was suggested for the M3/2-based sample. Results from the DTA also confirmed that carbon addition lowered some of the liquid-phase reaction temperatures. Measurement in M3/2-based material showed that the addition of 0.25% C reduced the first liquid-phase reaction temperature from 1050 to 1030 °C but had no effect on the upper 1090 °C reaction. Similar trends were noted when DTA curves were obtained under different atmospheres, notably that the substitution of nitrogen in place of argon as the protective gas in the DTA equipment also lowered the first liquid-phase reaction temperature.

3.3. Metallographic analysis

Specimens sintered at 720 °C were examined to establish the nature of the exothermic reaction produced at this temperature. Both the BT6 and M3/2 materials had undergone essentially similar reactions in that the copper phosphide powder particles added to the steel had reacted chemically with its surrounding steel matrix (Fig. 7). Energy-dispersive analysis showed that phosphorus had diffused into the steel to form a phosphorus-rich (phosphide) phase at the interface and that virtually pure copper (containing some dissolved iron) was left behind. The phosphide phase formed differed in composition for the two high-speed steel types (Table III).

Neither of these analyses corresponded to an exact M_3P phosphide compound, but the analysis technique could not detect any carbon which might have been present, and considerable scatter in the results for phosphorus concentration in different regions of the phosphide layer was caused by stray X-ray emissions from surrounding areas.

Further metallographic examinations were made to identify the liquid-phase reactions which had occurred during the sintering process. Sputter-coating of nital-etched specimens with iron oxide was used to identify phases by their colour on an optical microscope [2].

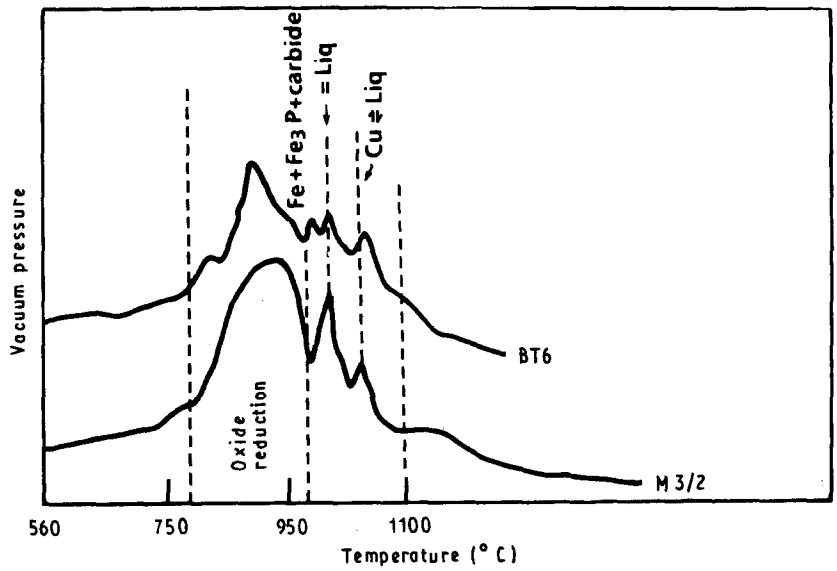

Figure 5 Vacuum pressure versus temperature during the sintering cycle: small pressure rises indicate the presence of liquid phase.

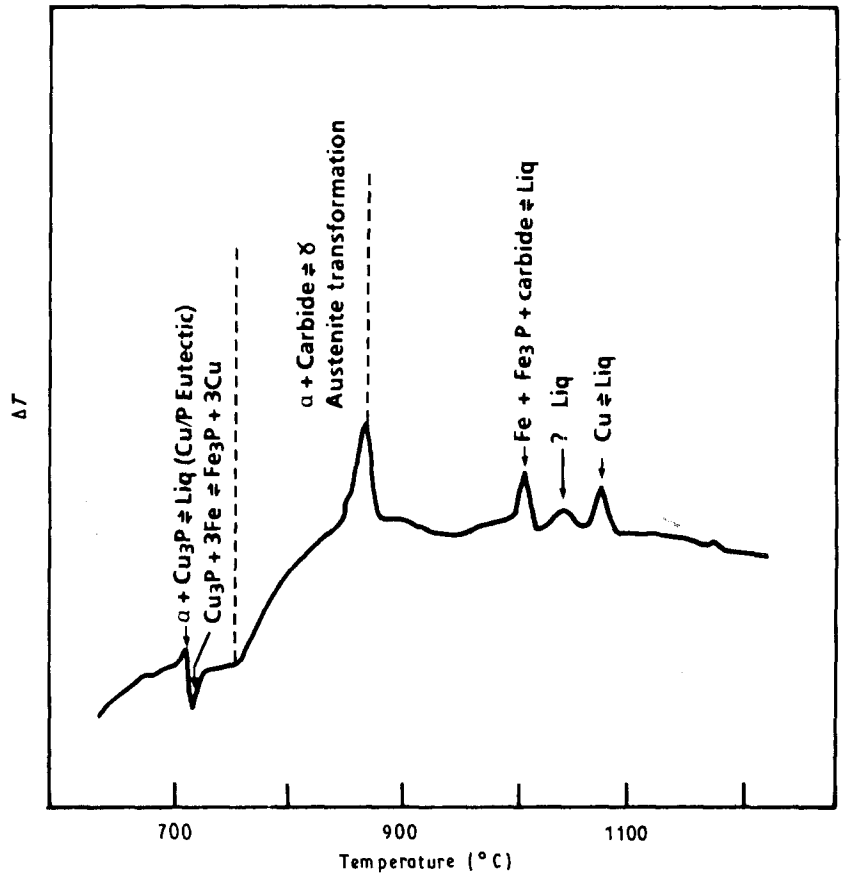

Figure 6 Thermal reactions shown by DTA curve for the heating of a BT6/copper–phosphorus alloy.

Energy-dispersive analysis and back-scattered electron contrast on a scanning electron microscope were also used to confirm phase identities and their compositions. Specimens sintered at temperatures near to the range where the first liquid phase was thought to occur revealed significant differences between the BT6 and M3/2 alloys. Clear evidence that a liquid phase had formed at temperatures where significant densification began, i.e. 1050 °C, was found in M3/2 specimens (Fig. 8), and this liquid had penetrated along prior austenite grain boundaries. The boundary film which remained after sintering was composed of a continuous layer of iron-rich phosphide and contained particles of MC and M_6C carbides. No such evidence of phosphide grain-boundary films was found in the BT6 materials sintered within the temperature range where liquid first began to appear (Fig. 9). Instead the structure showed that angular primary

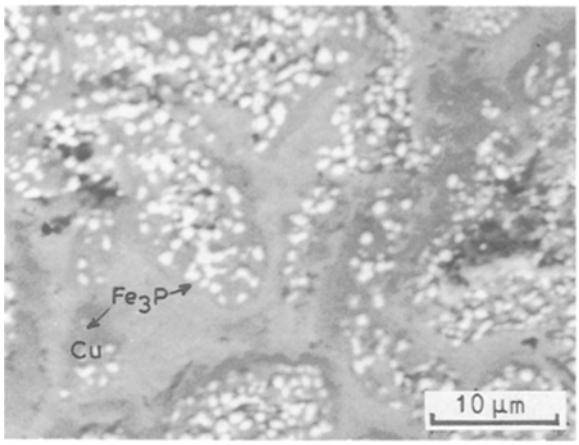

Figure 7 Microstructure of BT6 plus copper phosphide sintered at 720 °C. Molten copper–phosphorus eutectic liquid has flowed around the prior particles of H.S.S. and reacted to form an iron-rich M_3P phosphide and residual copper. Back-scattered electron image.

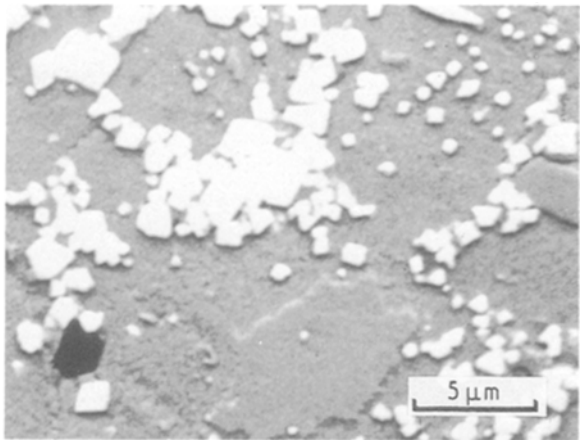

Figure 9 Microstructure of BT6 plus copper phosphide sintered at 1000 °C. Note the clusters of M_6C carbide which were embedded in a phosphide phase. Back-scattered electron image.

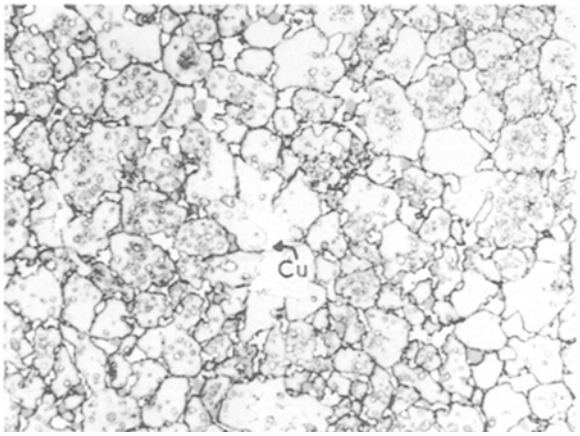

Figure 8 Microstructure of M3/2 plus copper phosphide sintered at 1070 °C. Note the suggestion of grain-boundary liquid from the presence of a phosphide film which also contained M_6C and MC carbides. × 1250. Sputter-coated with iron oxide.

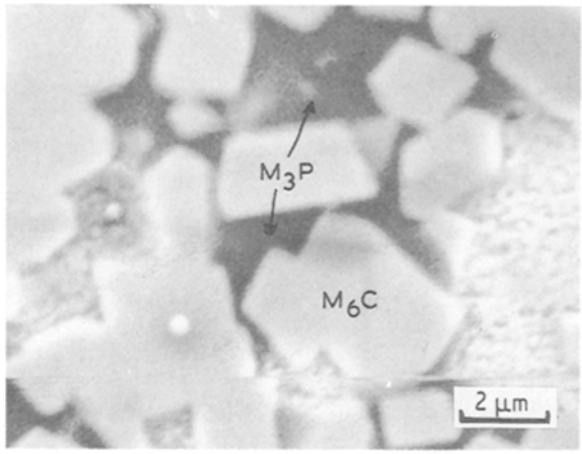

Figure 10 Carbide cluster formed in BT6/Cu–P material sintered at 1150 °C. Note the presence of iron-rich M_3P phosphide around the angular M_6C carbides. Secondary-electron image.

M_6C carbide particles were beginning to coarsen and to cluster together into agglomerated groups. Individual carbide particles within these groups were linked together by an iron-rich phosphide phase (Fig. 10). The iron-rich phosphide formed by these liquid-phase reactions differed in the two steel types and had compositions typical of those shown in Table IV.

As with the previous set of phosphide analysis results, no precise metal-to-phosphorus ratio which identifies the phosphide compound was found, but it was interesting to note how the phosphide phase had picked up more alloying elements from the steel compared with the phosphide formed at the lower temperature (see Table III).

Differences between the microstructures formed in BT6 and M3/2-based materials persisted at higher sintering temperatures, principally with regards to the morphology of the phosphide phase. The phosphide layer formed at prior austenite grain boundaries in M3/2 samples retained a similar composition at higher sintering temperatures, and herring-boned phosphide eutectic structures were found even at moderately high sintering temperatures well below those at which full density was achieved (Fig. 11). The actual eutectic structure also contained large angular M_6C

TABLE III Typical analysis for the phosphide formed at the steel–copper boundary at 720 °C

Alloy	Composition (at %)							
	Fe	Cr	Mo	W	V	Co	Cu	P
BT6	54.95	2.53	0.63	0.92	0.25	8.79	2.50	29.43
M3/2	62.05	2.66	0	0	0.40	–	5.46	29.42

TABLE IV Composition of the phosphide formed by liquid-phase reaction at temperatures near to the start of densification

Alloy	Composition (at %)							
	Fe	Cr	Mo	W	V	Co	Cu	P
BT6	41.48	13.85	1.24	2.65	3.02	11.87	0.75	25.14
M3/2	43.50	10.13	5.76	0.14	10.17	–	0.63	29.68

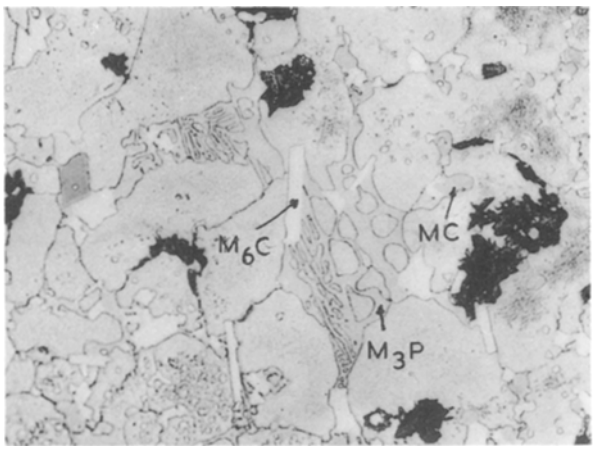

Figure 11 Typical herring-boned phosphide eutectic structure formed in M3/2 plus copper phosphide alloy. Sintered at 1120 °C. × 625. Sputter-coated with iron oxide.

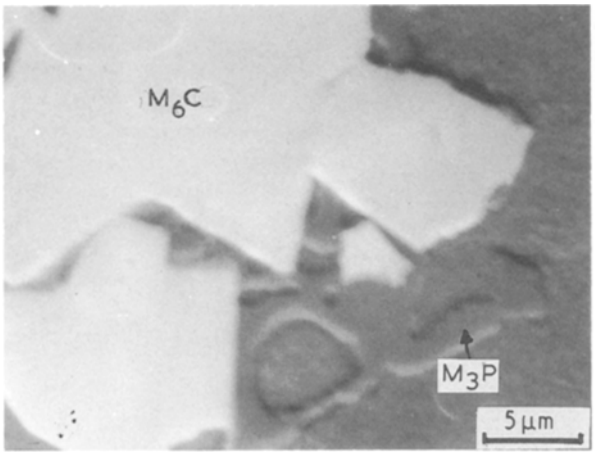

Figure 12 Phosphide eutectic structure formed by over-sintering in BT6 material. Sintered at 1230 °C. Back-scattered electron image.

carbides and more rounded vanadium-rich MC carbides; both types of carbide had obviously grown. Such eutectic structures were not detected in the BT6 materials until the material had been grossly over-sintered (Fig. 12). Instead, progressive coarsening of the M_6C carbides into clustered groups continued to develop as sintering temperatures were raised, until in the fully dense state stringer-like formations of coarse M_6C carbides occurred and the matrix was devoid of any smaller individual carbide particles. The phosphide phase continued to form a cementing layer between the carbides within the carbide cluster (see Fig. 10), and also did not change significantly in composition from that shown in Table IV. No vanadium-rich MC carbides were detected in any of the BT6-based alloys.

In both types of high-speed steel there was also evidence that the carbides formed in association with any phosphide phase also differed from those found in normal high-speed steels. The M_6C carbides, for instance, contained significant quantities of phosphorus, whereas the vanadium-rich MC-type carbides found in M3/2 steel eutectic structures did not contain phosphorus but did contain a higher than expected vanadium content.

Some differences in microstructure were produced by the addition of extra carbon before sintering and when either vacuum or nitrogen-atmosphere sintering was used. Furnace-cooling from the sintering temperature after vacuum sintering produced predominantly martensitic matrices in the M3/2 materials and a mixed pearlite plus martensite structure in the BT6 alloys. In both cases carbon addition increased the amount of pearlite formed in the as-vacuum-sintered structure. Nitrogen-atmosphere sintering also increased the tendency for pearlite to form in the as-sintered structure for both types of high-speed steel, but produced little other change except in the M3/2 alloys. Within the M3/2 alloys the elemental compositions of the M_6C carbides changed very little with either carbon addition or with the change from vacuum to nitrogen-atmosphere sintering, but the vanadium-rich MC carbides appeared to become enriched in vanadium and depleted in both molybdenum and tungsten by nitrogen-atmosphere sintering.

Finally, chemical analysis was performed to check whether nitrogen-atmosphere sintering had in fact led to the absorption of nitrogen into the sample during sintering. The figures suggested that no nitrogen absorption occurred for materials sintered under a partial pressure of nitrogen, but considerable nitrogen absorption occurred when sintering was performed with nitrogen at full atmospheric pressure, i.e. an increase from 0.01 to 0.16 wt % N.

4. Discussion

4.1. Liquid-phase sintering due to phosphorus addition

In conventional high-speed steel powder metal processing, without the addition of sintering aids, densification occurs by a liquid-phase mechanism formed by a super-solidus reaction: liquid phases are formed when the steel is heated to within the liquidus–solidus temperature range inherent in the standard high-speed steel alloy composition being processed [3, 4]. The standard sintering practice needed to form fully dense samples in either M3/2 or BT6 grade high-speed steels would require sintering temperatures within the region of 1250 and 1310 °C, respectively. The results shown in Figs 1 and 2 indicate that sintering to near-full density was achieved at much lower temperatures than these for both types of steel because of the introduction of copper–phosphorus alloy powder: M3/2 was fully dense at 1140 °C and BT6 at around 1180 °C. Previous work has already established the essential mechanisms by which copper–phosphorus assists densification, at least in M3/2 alloys [2], and it was concluded that a type of activated liquid-phase sintering was involved. Several liquid-phase reactions were involved and stemmed from the reaction between copper phosphide (Cu_3P) and its surrounding steel matrix. Initially the copper–phosphorus reacted to form an iron-rich phosphide compound, recently identified as an M_3P-type compound [5], and pools of copper were left as a residual product. Transient liquid phases were formed at a succession of different sintering temperatures and sharp increases in densification

rate occurred at each reaction temperature. The suggested reactions were

(i) a eutectic reaction of iron phosphide (Fe_3P) + carbide + either ferrite or austenite, at around 1050 °C;

(ii) melting of residual copper, left by the earlier chemical reaction, at around 1090 °C; and

(iii) a super-solidus eutectic, austenite + M_6C carbide, at around 1150 °C.

A model was also proposed which suggested that the liquid phase formed at prior austenite grain boundaries by the phosphide eutectic promoted densification through an increase in grain growth rate caused by solution and re-precipitation of carbides across the grain-boundary liquid phase region [2].

Changes in densification rate with each successive liquid-phase reaction can also be seen on the sintering curves shown in Figs 1 and 2, but the reaction temperatures were different for the two steels. Densification due to vacuum sintering with no additional carbon starts in BT6 alloy at a somewhat lower temperature than in M3/2 material; densities started to increase significantly at around 990 °C in BT6 alloy and only at about 1040 °C in the M3/2 alloy. In spite of the lower start temperature for densification in the BT6 material, higher temperatures were required to achieve near-full density than in the M3/2 alloys, possibly due to the need to achieve a higher overall density, e.g. 8.95 instead of 8.2 $g\,cm^{-3}$.

Copper–phosphorus addition thereby seems to be producing similar liquid-phase sintering reactions in both the BT6 and M3/2 alloys. A chemical reaction between the copper phosphide and the steel occurred in both steels, and an iron-rich Fe_3P phosphide was produced which contained some of the alloying elements found in the steel matrix, notably cobalt in the BT6 alloy (see Table III). The products of this reaction caused a series of liquid-phase reactions, whose existences were confirmed by DTA and by the gas evolution results, which produced changes in densification rate at different sintering temperatures. There were, however, distinctive differences between the behaviours of the two type of high-speed steel concerning the development of sintered microstructure and in the reaction temperatures.

The M3/2 alloys followed a sequence of transient liquid-phase sintering reactions of the type already documented [2], where sintering began at approximately 1040 °C due to the formation of liquid as the product of an iron + phosphide + carbide eutectic similar in many respects to that encountered in high-phosphorus cast iron. Earlier work [2, 6] suggested that ferrite was the participant phase in this eutectic, but austenite may also take part. At higher temperatures, i.e. at approximately 1090 °C, the melting of copper also provides a further means of liquid-phase sintering by which the second densification stage occurs. At the final stage, at above 1150 °C, phosphorus dissolved in the M_6C carbides brings down the super-solidus sintering temperature so that liquid can form by an austenite plus M_6C carbide eutectic reaction.

Some insight into the actual sintering mechanisms for M3/2 was obtained from the sintering data shown in Fig. 4, in that the Kingery slopes indicated both a solution–reprecipitation and a particle rearrangement process [7], depending upon the sintering temperature. The curves shown in Fig. 4 do not show all three stages of the classical liquid-phase sintering model at one sintering temperature because of the slow heating rates used to determine these results. Slow heating rates (10 °C min^{-1}) were necessary in order to protect the furnace ceramic tube from thermal shock, and meant that densification had already progressed to some extent before a constant sintering temperature was reached; isothermal measurements could have missed the earlier reaction stages. Nevertheless the major reaction at low sintering temperatures, e.g. when the phosphide eutectic liquid first begins to appear at 1050 °C, appeared to be particle rearrangement and metallographic evidence supported this idea. The phosphide eutectic liquid could be seen at prior particle boundaries and more importantly at prior austenite grain boundaries (Fig. 8). Penetration along prior austenite grain boundaries by the phosphide-rich liquid would encourage densification by particle rearrangement due to capillary liquid forces along prior austenite grain boundaries. At higher sintering temperatures, e.g. 1120 °C, solution and reprecipitation became the more dominant densification mode, possibly via the grain growth mechanism previously referred to. Additional evidence now suggests, however, that solution of the steel matrix into the phosphide-rich liquid followed by the reprecipitation of alloying elements on to carbides may also occur; note the observed growth of carbide particles in Fig. 11, and the solution of alloying elements (vanadium, chromium and molybdenum) into the phosphide phase (see Table IV).

Although densification also occurred in stages due to successive liquid-phase formation in BT6 alloys, the reactions appeared to be more complex and were less easily identified than those seen in M3/2 alloys. At approximately 1090 °C melting of residual copper, left from the chemical breakdown of copper phosphide, also contributed towards densification, as in the M3/2 steels, but at temperatures below this there appeared to be two liquid-phase reactions rather than one, i.e. at 990 and 1040 °C. Metallographic observations were unable to distinguish whether two liquid phases were actually formed at these temperatures, and neither was there evidence of any eutectic structure. Whatever the reactions were there was evidence that clustered groups of M_6C carbides, surrounded by an iron-rich M_3P phosphide phase, were formed and that the reaction produced at the lower of the above temperatures might be consistent with the reaction iron + Fe_3P + M_6C = liquid. The second of the above two reaction temperatures might correspond to a psuedo-binary reaction between M_6C carbide and the more highly alloyed iron-rich M_3P phosphide formed by the dissolution of steel into the phosphide phase, but there was little positive microstructural evidence other than the existence of clusters of M_6C carbides surrounded by phosphide phase to support this idea.

Metallographic evidence and the sintering kinetic data shown in Fig. 3 also suggested that a solution–reprecipitation process was largely responsible for densification in the BT6 materials. The apparent absence of phosphide films at prior austenite grain boundaries and the data found by Kingery slope analysis indicated that liquid-assisted particle rearrangement along prior austenite grain boundaries made a seemingly less important contribution towards densification in BT6 than in the M3/2 alloys. Solid-state diffusion also made a significant contribution to sintering at higher temperatures in place of the super-solidus sintering found for the M3/2 alloys.

The solution–reprecipitation mechanism most in accord with metallographic evidence suggested that liquid phase was formed at around 990 °C by melting between the steel matrix and an iron-rich M_3P phosphide. This liquid penetrated around prior particle boundaries and dissolved away some of the steel matrix so that some small undissolved M_6C carbide particles were picked up by the liquid from the original high-speed steel powder. The M_6C carbide particles were swept into pore zones which lay between prior particles by the flow of liquid and formed clustered groups where they acted as nuclei for growth into larger carbide particles; solution of the steel into the phosphorus-rich liquid and the transport of alloying elements through this liquid phase into the carbide clusters caused growth of the carbides by reprecipitation from the liquid phase.

Changes in the composition of the various liquid phases as the sintering process progressed could be responsible for the transient behaviour observed for both steels. Carbon depletion in the phosphorus-rich liquid as the result of carbide growth would contribute towards the eventual isothermal solidification of this liquid. Mutual solution and exchange between copper and iron would also eventually exhaust any contribution made to densification made by molten copper.

4.2. The effects of added carbon and nitrogen on sintering behaviour

Carbon additions are known to reduce the temperatures required for super-solidus sintering in conventional high-speed steel powder metallurgy [8–10], principally because of two effects. Firstly, chemical reduction of surface oxides from the powder particle surfaces by the formation of carbon monoxide can assist the sintering process [10], and secondly carbon is known to lower the solidus temperatures in high-speed steels with the effect of creating a liquid-phase sintering reaction at lower than normal temperatures.

Nitrogen has an equivalence with carbon; it too forms an interstitial solid solution with high-speed steels, and can also reduce sintering temperatures, as well as forming carbonitrides in place of the MC carbide phase [11–14].

The current work, of course, does not strictly relate to super-solidus sintering except at the upper temperature range, but our own experimental evidence together with that of other co-workers [15] clearly indicates that the liquid reaction, involving iron-rich phosphide phases and responsible for initial densification, was depressed to a lower temperature by adding either carbon or nitrogen. Carbon additions were more effective in lowering the initial sintering temperatures for M3/2 than for BT6 alloys, and produced a greater increase in density for this initial stage by encouraging more of the phosphide-rich liquid phase to form. Carbon was also probably effective in enhancing densification due to the final stage, of austenite plus carbide eutectic at above 1150 °C, especially in the M3/2 material. As should be expected, little change occurred in the mid-sintering temperature range where the formation of copper-rich liquid was predominant.

The effects of nitrogen-atmosphere sintering on densification were inconclusive and seemed to produce no marked effects. This lack of effect was, however, almost certainly linked to the fact that no nitrogen was absorbed from nitrogen atmospheres at partial pressures. Some oxidation and possibly decarburization also occurred at atmospheric nitrogen pressures, which may have counteracted any beneficial effects that nitrogen might have produced. The only change brought about by a nitrogen atmosphere was the apparent change in vanadium content for MC carbides in the M3/2 material, which might support claims for the formation of carbonitrides in place of the MC carbides in M3/2 materials [11]. The M_6C carbides appeared to be unaffected by nitrogen atmospheres.

5. Conclusions

1. Copper–phosphorus additions reduce the temperatures required to produce near-full density in sintered high-speed steels. Iron-rich M_3P phosphides are produced by reaction between the copper phosphide and its surrounding steel, and the products of this reaction lead to a series of liquid phases which promote liquid-phase sintering in a succession of different reactions, namely

(a) iron-rich M_3P phosphide + iron + carbide = liquid;

(b) melting of residual copper; and

(c) formation of super-solidus eutectic liquid from a carbide plus austenite eutectic.

2. Greater reductions in sintering temperature were achieved by adding copper phosphide to BT6 alloys than were achieved for M3/2, but higher overall temperatures were required to produce near-full density in the BT6 alloys.

3. Carbon addition lowered the temperature required both to initiate and to complete densification in both types of steel, but was more effective in M3/2 than in BT6 steels.

4. Nitrogen-atmosphere sintering did not produce the hoped-for reductions in sintering temperature, despite evidence that interstitial nitrogen was capable of being absorbed and of reducing the temperature for the phosphide eutectic. Oxidation due to contamination of the nitrogen atmosphere or insufficient pressure of nitrogen were the main culprits for giving inconclusive results.

5. The addition of copper–phosphorus and extra carbon to high-speed steel before sintering is capable of reducing the sintering temperature to a level compatible with continuous link belt furnace operation.

References

1. W. D. KINGERY, *J. Appl. Phys.* **30** (1959) 301.
2. J.D. BOLTON, C. JOUANNY TRESY and M. JEANDIN, *Powder Metall.* **33** (1990) 126.
3. C. S. WRIGHT, *ibid.* **32** (1989) 114.
4. R. M. GERMAN, *Int. J. Powder Metall.* **26** (1990) 23.
5. C. JOUANNY-TRESY, M. JEANDIN, N. De DAVE and J. MASSOL, in Conference Proceedings, "Controlling Properties in Powder Metallurgy Parts Through Microstructure" Paris, France, 1990. (Société Francais de Metallurgia, Paris, 1990) p. 14.
6. W. F. JANDESKA, *Progr. Powder Metall.* (1981) 233.
7. R. M. GERMAN, S. FAROOQ and C. M. KIPPHUT, *Mater. Sci. Engng* **A105/106** (1988) 215.
8. R. WAHLING, P. BEISS and W. J. HUPPMAN, *Powder Metall.* **29** (1986) 53.
9. K. M. KULKARNI, A. ASHURST and M. SVILAR, *Mod. Devel. Powder Metall.* **13** (1981) 93.
10. W. J. PRICE, M. M. REBBECK A. S. WRONSKI and A. S. AMEN, *Powder Metall.* **28** (1985) 1.
11. A. H. PALMA, V. MARTINEZ and J. J. URCOLA, *ibid.* **32** (1989) 291.
12. H. S. NAYER, *Progr. Powder Metall.* **33** (1977) 197.
13. R. M. GERMAN and K. A. D'ANGELO, *Int. Met. Rev.* **29** (1984) 249.
14. M. HIRANO and N. KAWAI, *Met. Powder Rep.* **41** (1986) 527.
15. M. OLIVEIRA, private communication, L.N.E.T.I., Lisbon, Portugal (1989).

Received 13 August 1990
and accepted 9 January 1991